JEM Journal of Experimental Medicine

BRIEF DEFINITIVE REPORT

Gain-of-function *IKBKB* mutation causes human combined immune deficiency

Chelisa Cardinez[1,2,3*], Bahar Miraghazadeh[1,2,3*], Kay Tanita[4*], Elizabeth da Silva[2], Akihiro Hoshino[4], Satoshi Okada[5], Rochna Chand[1,2,3], Takaki Asano[5], Miyuki Tsumura[5], Kenichi Yoshida[6], Hidenori Ohnishi[7], Zenichiro Kato[7,8], Masahide Yamazaki[9], Yusuke Okuno[10], Satoru Miyano[11,12], Seiji Kojima[13], Seishi Ogawa[6], T. Daniel Andrews[1,3], Matthew A. Field[1,3,14], Gaetan Burgio[3], Tomohiro Morio[4], Carola G. Vinuesa[1,3], Hirokazu Kanegane[4], and Matthew C. Cook[1,2,3]

Genetic mutations account for many devastating early onset immune deficiencies. In contrast, less severe and later onset immune diseases, including in patients with no prior family history, remain poorly understood. Whole exome sequencing in two cohorts of such patients identified a novel heterozygous de novo *IKBKB* missense mutation (c.607G>A) in two separate kindreds in whom probands presented with immune dysregulation, combined T and B cell deficiency, inflammation, and epithelial defects. *IKBKB* encodes IKK2, which activates NF-κB signaling. IKK2^{V203I} results in enhanced NF-κB signaling, as well as T and B cell functional defects. IKK2^{V203} is a highly conserved residue, and to prove causation, we generated an accurate mouse model by introducing the precise orthologous codon change in *Ikbkb* using CRISPR/Cas9. Mice and humans carrying this missense mutation exhibit remarkably similar cellular and biochemical phenotypes. Accurate mouse models engineered by CRISPR/Cas9 can help characterize novel syndromes arising from de novo germline mutations and yield insight into pathogenesis.

Introduction

More than 300 single-gene defects that result in immunological disease have been described so far (Picard et al., 2018). Elucidation of Mendelian immune diseases is important for the families affected and, in some cases, provides insights into disease mechanisms that are of broader therapeutic significance for autoimmunity and lymphoproliferative disease (Woyach et al., 2012). Among the known causes are many homozygous and biallelic loss-of-function alleles that result in devastating early onset immunological disease. In addition, there is an emerging catalog of single-gene defects that result in much less severe phenotypes, and some of these syndromes share significant similarities with diseases assumed to be the result of polygenic variation.

Mutations that result in defective NF-κB signaling and transcription are exemplary. NF-κB is a family of transcription factors that regulate gene expression in many tissues and exert important and well-characterized actions on lymphocyte ontogeny, homeostasis, activation, and maintenance of self-tolerance (Zhang et al., 2017). In the resting state, NF-κB molecules are retained in latent form in the cytoplasm by molecules of the IκB family (Baeuerle and Baltimore, 1988). After receptor ligation, signals converge on a complex comprising IKK1, IKK2, and NEMO (encoded by *IKBKA*, *IKBKB*, and *IKBKG*, respectively), which phosphorylates IκBα, targeting it for partial degradation in the proteasome, which liberates NF-κB molecules p65 (RelA), c-Rel, and p50 (Fan and Maniatis, 1991; Salmerón et al., 2001; Häcker and Karin, 2006; Scheidereit, 2006) to the nucleus as transcription factors (Plaksin et al., 1993; Weih et al., 1995; Bohuslav et al., 1998; Hayden and Ghosh, 2004). Many germline NF-κB defects

[1]Centre for Personalised Immunology, Australian National University, Canberra, Australia; [2]Department of Immunology Canberra Hospital, Canberra, Australia; [3]Department of Immunology and Infectious Diseases, John Curtin School of Medical Research, Australian National University, Canberra, Australia; [4]Department of Child Health and Development, Graduate School of Medical and Dental Sciences, Tokyo Medical and Dental University, Tokyo, Japan; [5]Department of Pediatrics, Hiroshima University Graduate School of Biomedical and Health Sciences, Hiroshima, Japan; [6]Department of Pathology and Tumor Biology, Graduate School of Medicine, Kyoto University, Kyoto, Japan; [7]Department of Pediatrics, Gifu University Graduate School of Medicine, Gifu, Japan; [8]Structural Medicine, United Graduate School of Drug Discovery and Medical Information Sciences, Gifu University, Gifu, Japan; [9]Department of Internal Medicine, Keiju Medical Center, Nanao, Japan; [10]Center for Advanced Medicine and Clinical Research, Nagoya University Hospital, Nagoya, Japan; [11]Laboratory of DNA Information Analysis, Human Genome Center, Institute of Medical Science, The University of Tokyo, Tokyo, Japan; [12]Laboratory of Sequence Analysis, Human Genome Center, Institute of Medical Science, The University of Tokyo, Tokyo, Japan; [13]Department of Pediatrics, Nagoya University Graduate School of Medicine, Nagoya, Japan; [14]Australian Institute for Tropical Health and Medicine, James Cook University, Cairns, Australia.

*C. Cardinez, B. Miraghazadeh, and K. Tanita contributed equally to this paper; Correspondence to Matthew Cook: matthew.cook@anu.edu.au; Hirokazu Kanegane: hkanegane.ped@tmd.ac.jp.

have been identified as causes of immunological disease. In some cases, for example, *CARD11*, biallelic mutations cause early onset disease, while heterozygous variants cause different phenotypes (Snow et al., 2012; Stepensky et al., 2013). Interestingly, somatic mutations in many of the same NF-κB genes have also been implicated in lymphoproliferative disease (Staudt, 2010).

Now that there is empirical evidence that single-gene variants can cause complex immune phenotypes, it is important that we explore rare and novel variants in cases where disease remains unexplained. De novo mutations are an important cause of severe sporadic disease with immunological and other phenotypes (Vissers et al., 2010; Conley and Casanova, 2014; Flanagan et al., 2014), although in such cases, opportunities for proving causation by segregation analysis are usually limited. In addition, the catalog of variants of unknown significance is large. In both cases, methods for determining function of precise human mutations that might account for a novel syndrome is a high priority. Here, we report how combined phenotyping of patients carrying a de novo gain-of-function mutation in *IKBKB*, and a mouse engineered to carry the orthologous variant, helped to describe a novel immune syndrome.

Results and discussion

We assembled a cohort of patients with noncongenital immune deficiency, manifesting as either primary antibody deficiency, unexplained T cell deficiency, or various combined defects. From within this cohort we identified a patient who presented with recurrent respiratory tract infections, severe and atypical eczema, dental abnormalities consistent with ectodermal dysplasia (without conical teeth), hidradenitis suppurativa and subcutaneous abscesses, mucocutaneous candidiasis, and premature cataracts. Both parents were alive with no evidence of immune deficiency or dysregulation. The proband had two children (aged 2 and 5 yr), and both suffered with recurrent otitis media and sinusitis, but no inflammation or ectodermal dysplasia. Initial cellular analysis of peripheral blood mononuclear cells (PMBCs) isolated from the proband and both children revealed lymphopenias. One child, from whom blood was available for analysis, and the proband both exhibited T deficiency, and the other exhibited a reduction in total lymphocytes for age. Lymphopenia was a fixed phenotype in the proband, with no significant change over at least 7 yr of observation (Table S1). In addition, she had mild hypogammaglobulinemia and defective specific antibody responses to pneumococcal vaccination.

Whole exome sequencing and analysis of kindred A using methods described previously (Field et al., 2015) identified a novel heterozygous missense mutation in *IKBKB* (c.607G>A, cDNA.793G>A, g.37639G>A) encoding a valine to isoleucine (V203>I) amino acid substitution (Fig. 1, a and b). No other rare or novel mutations were identified in genes encoding NF-κB proteins. The *IKBKB* mutation was not found in either parent, and after excluding nonpaternity with high confidence, we concluded that the mutation had arisen de novo in the proband. An identical codon variation was discovered in a separate and geographically remote kindred (Fig. 1, a and b), involving a 33-yr-old male proband with a history of recurrent respiratory infections, otitis media, and tonsillitis since childhood. He was noted to have hypogammaglobulinemia at age 18 yr and subcutaneous abscesses at age 28 yr. Further investigations revealed bronchiectasis (Fig. 1 c) and hepatosplenomegaly (Table S1).

Valine 203 is conserved to at least *Drosophila melanogaster* (Fig. 1 d), is located within the active site of IKK2 (Fig. 1, e and f), on the second lobe of the kinase domain, which phosphorylates the N-terminal region of IκBα, and leads to activation of NF-κB (Liu et al., 2013). The mutant protein is predicted to assume an unstable conformation, while maintaining the kinase activity, but disrupting the tetrameric interaction of IKK2. The mutated residue is conserved in protein paralogs of IKK2 (Fig. S1 a). In silico analysis predicted the mutation to be damaging (SIFT, 1.0; Polyphen2, 0.99; Mutation Taster, >0.99). This germline mutation has not been reported before (GnomAD, ExAC, dbSNP), but two instances of the same mutation arising as a somatic variant in brain tumors have been reported (Fukumura et al., 2016). Consistent with our findings, this somatic variant was reported to confer gain of function. Thus, we report a novel syndrome of combined immune deficiency arising from germline gain-of-function *IKBKB* mutations.

Flow cytometric analysis showed that IKK2 protein was expressed at similar levels in patient and control lymphocytes (Fig. S1 b). We proceeded to analysis of the mutant allele. First, we cloned mutant and WT alleles and expressed them in HEK293 cells. After stimulation with TNF, we observed increased and prolonged IκBα phosphorylation, despite similar levels of WT and mutant allele IKK2 expression (Fig. 1 g). Similarly, we observed increased IκBα phosphorylation at baseline and after activation of PBMCs obtained from the proband (Fig. S1, c and d).

IKK2 activates the canonical NF-κB pathway. We examined the effect of the mutation by assessing abundance of phosphorylated p65 in fibroblasts, T and B cells at rest, and after activation (Fig. 1, h and i; and Fig. S2 a). As had been observed for the proximal event (phospho-IκBα), we observed increased phospho-p65, particularly in the T cell compartment, and an increase in abundance of phospho-p65 after activation out to 60 min (Fig. 1 h). Non-stimulated B cells from the patient showed increased phosphorylation of NF-κB to a level similar to that in CD40-stimulated control B cells (Fig. S2, b and c), with an enhanced response to PMA plus ionomycin and CD40 ligand plus IL-4 (Fig. S2, d and e).

We also assessed the transcriptional consequences of enhanced NF-κB activation. First, dendritic cells were induced in vitro from monocyte precursors. NF-κB2 is under transcriptional control by canonical NF-κB signaling, and while baseline expression was similar in patient and control, we observed an increase in patient cells after activation in vitro with TNF (Fig. S1, e and f). To demonstrate transcriptional regulation, we transfected fibroblasts isolated from patient and a healthy control with a construct containing NF-κB–dependent luciferase. We observed a modest increase in NF-κB–dependent transcription in the absence of stimulation and a significant increase relative to control after activation (Fig. 1 i). We performed a similar analysis after transient transfection of HEK293T cells with either WT, $IKBKB^{V203I}$, $IKBKB^{R272X}$ (a known hypomorphic allele), or $IKBKB^{K171E}$ (a known gain-of-function allele; Fig. 1 j; Kataoka et al., 2015). Even in the absence of stimulation, $IKBKB^{V203I}$ resulted in enhanced

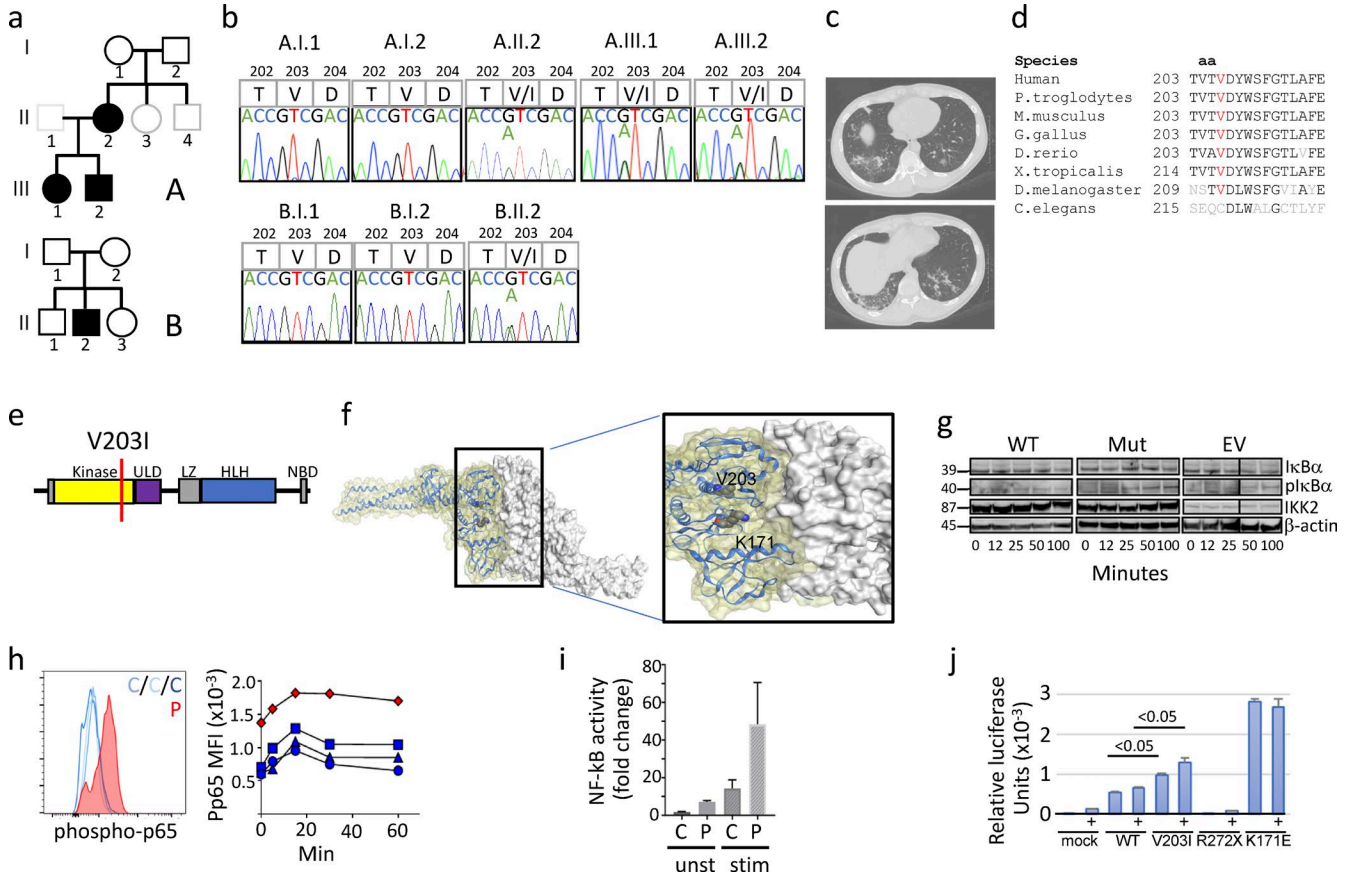

Figure 1. **Novel *IKBKB* mutation. (a)** Pedigree. Affected (filled symbols) and unaffected (unfilled symbols). Gray symbols, not genotyped. **(b)** Sanger sequencing of family members, as indicated by pedigree. Translated amino acids are indicated by single letter code (T, threonine; V, valine; I, isoleucine; D, aspartate). **(c)** Chest computerized tomography reveals bronchiectasis in middle and lower lobes in B.II.2. **(d)** Phylogeny of mutated residue (valine 203, red). **(e)** Schematic of IKK2 protein to indicate location of p.V203>I mutation. ULD, ubiquitin-like domains; LZ, leucine zipper; HLH, helix-loop-helix; NBD, NEMO binding domain. **(f)** Ribbon diagram of IKK2 (PDB code: 4KIK) with substituted amino acid (red) shown within the activating pocket in the kinase domain. **(g)** Immunoblot for IκBα, phospho-IκBα (pIκBα), and total IKK2 and on lysates from HEK293 cells transfected with WT or mutant (Mut) *IKBKB* constructs or empty vector (EV). Molecular weights (kD) shown. Representative of three experiments. **(h)** Expression of phospho-p65 in T cells from patient (blue histogram) and three unrelated controls (red histograms). Representative of three experiments. **(i)** Increased NF-κB–dependent transcription according to luciferase activity in fibroblasts obtained from patient (A.I.2) and controls in the presence or absence of activation with TNF. Representative of three experiments. **(j)** NF-κB reporter activity in HEK293T cells transfected with IKBKB constructs (as indicated), unstimulated or stimulated (+) with TNF. P values shown, Student's *t* test.

luciferase activity compared to the WT allele, and this response was enhanced after TNF stimulation.

Probands in both kindreds exhibited deficiencies of $CD4^+$ and $CD8^+$ T cells, with a significant reduction in naive T cells in both compartments (Fig. 2, a and b; naive $CD4^+$ T cells, A.II.2: 4.19%; B.II.2: 17.4%. Naive $CD8^+$ T cells, A.II.2: 4.93%; B.II.2: 6.9%). Indeed, this deficiency was observed in both αβ and γδ T cells (data not shown). We also observed a significant increase in circulating follicular helper T cells (Tfh cells; Fig. 2, c and d). Consistent with an effector memory T cell (T_{EM})/T_{EM} $CD45RA^+$ cell (T_{EMRA}) phenotype, patient $CD8^+$ T cells showed increased expression of CD107a, a degranulation marker (Fig. S2 f).

The probands were also found to exhibit a significant deficiency of memory B cells (Freiburg class Ib), defined either as $CD19^+IgD^-CD27^+$ (Fig. 2, e and f; and Table S1) or $CD19^+CD38^{lo}CD24^{hi}$ lymphocytes (Fig. S2 g). Transitional B cells were numerically normal, but were universally $CD21^{hi}CD10^+$ (Fig. S2 h). Analysis of IgD^+CD19^+ B cells revealed a relatively low level of IgM expression, a phenotype often observed as a result of a reduced threshold of B cell receptor activation (Fig. S2 i). We observed a modest reduction in CD86 induction by both naive and memory B cells after activation with bacteria cytidine-phosphate-guanosine (CpG), while induction of CD25, CD83, and CD69 was normal (data not shown). B cells failed to proliferate normally and exhibited a defect in immunoglobulin production after CD40 or CpG stimulation (Fig. 2, g and h).

We purified naive and memory T cells and assessed their responses to activation in vitro. We observed similar proliferation responses by memory T cells ($CD45RO^+$) from proband and controls (Fig. 3 a). In contrast, activation of naive $CD4^+$ T cells from the proband responded with greater proliferation relative to those from unrelated healthy controls. Activation of naive cells was accompanied by increased expression of markers of activation CD25 and CD69 (Fig. 3, a and b). To confirm the enhanced proliferative response in cells from the proband, we stimulated cells with CD3 only (rather than CD2, CD3, and CD28), which normally induces only a small proportion of cells to enter cycle, and observed a substantial proliferative response in cells from the

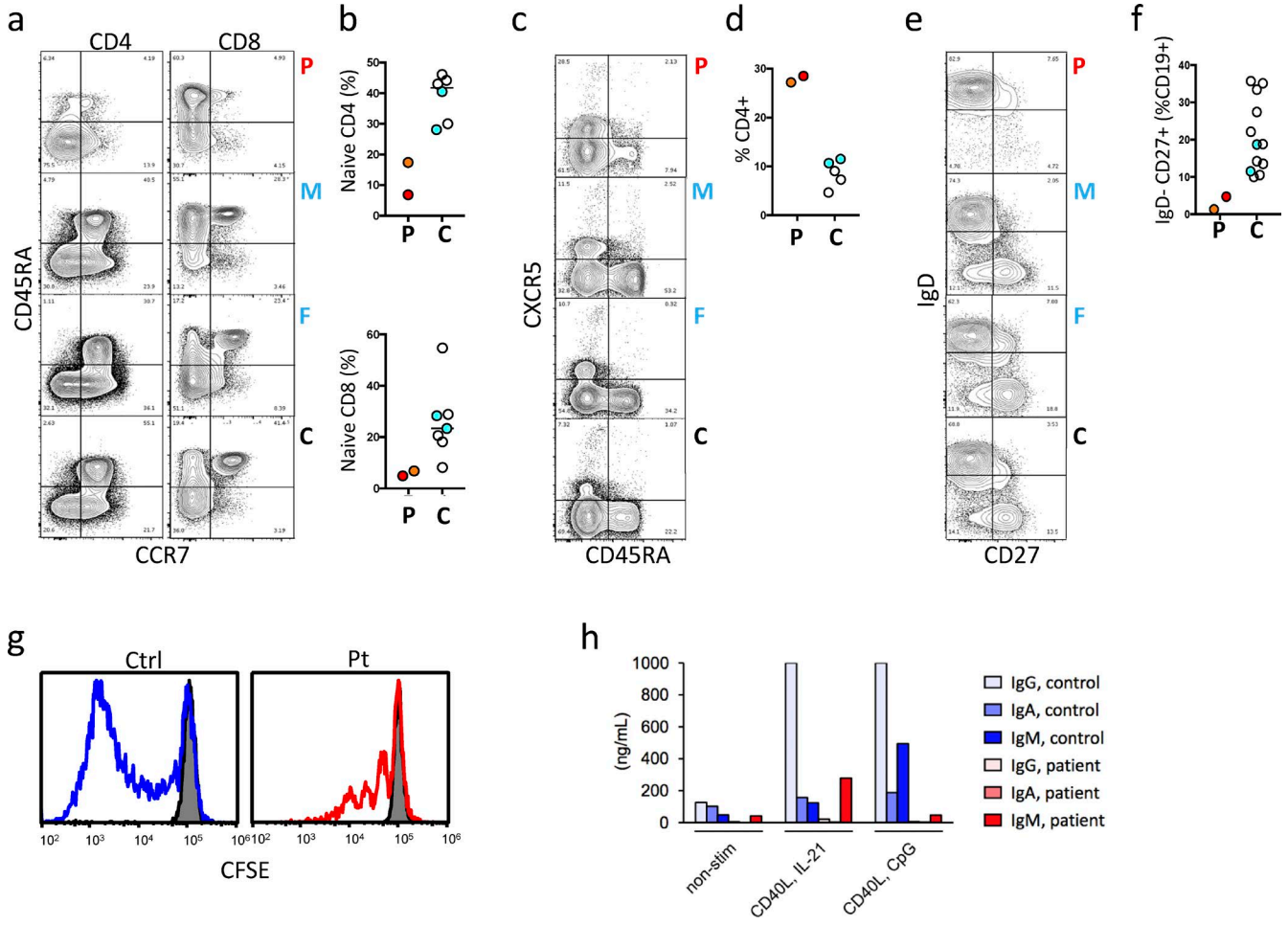

Figure 2. **Phenotyping of peripheral blood mononuclear cells. (a)** Analysis of T cell compartments, naive ($CCR7^+CD45RA^+$), central memory ($CCR7^+CD45RA^-$), $CD45RA^+$ effector memory (T_{EMRA}; $CCR7^-CD45RA^+$), and conventional effector memory ($CCR7^-CD45RA^-$). Representative profile is shown for proband, mother, father, and healthy control. Representative of two experiments. **(b)** Summary data of naive T cells gated on $CD4^+$ or $CD8^+$. **(c)** Analysis of circulating Tfh ($CXCR5^+CD45RA^-$) gated on $CD4^+$ T cells. Representative of two experiments. **(d)** Summary data of Tfh cells analysis. **(e)** Analysis of B cell subsets gated on $CD19^+$ cells. Non-switched memory ($CD27^+IgD^+$), switched memory ($CD27^+IgD^-$), and naive ($CD27^-IgD^+$). Representative of four experiments. **(f)** Summary data percentage of $CD19^+$ cells analyzed for memory B cells. In each summary plot, for patients (red, A.II.2; orange, B.II.2), parents (blue), and healthy controls (open symbols). Representative of two experiments. **(g)** Proliferation assay of $CD20^+$ B cells using CSFE after CD40 and CpG stimulation. **(h)** In vitro immunoglobulin production by PBMCs. C, healthy control; F, father; M, mother; P, proband.

proband, but not in controls (Fig. 3 c). In these proliferation assays, although we observed an enhanced proliferative response, there were far fewer cells present in cultures at time of analysis, consistent with substantial cell death.

We also observed a significant increase in circulating regulatory T cells (T reg cells) in A.II.2, but not in B.II.2, defined as $CD25^+CD127^-$ and $FOXP3^+$, and effector T reg cells, defined as $CD45RA^-$, $FOXP3^+CD25^+$, and $CD127^-$ (Fig. 3, d and e). Interestingly, we also observed an increase in FOXP3 expression per cell, which was evident within T reg cells and also in the otherwise low-level FOXP3 expression in $CD4^+$ T cells considered to be conventional T cells by surface phenotype (Fig. 3, f and g).

$IKK2^{V203}$ is highly conserved across species and in similar proteins (Fig. 1 d and Fig. S1 a), so to investigate the action of this novel germline mutation in vivo, and to confirm its causal action in immune dysregulation, we engineered a G-to-A transversion in codon 203 of mouse *Ikbkb* using CRISPR/Cas9 (Fig. 4 a). The mutant allele was propagated, and heterozygous and homozygous mice were born at expected Mendelian ratios.

Analysis of isolated splenocytes revealed constitutive IκBα phosphorylation, with evidence of a gene dose effect: phosphorylation was greater in cells with homozygous mutation compared with heterozygotes, both at baseline (Fig. 4 b) and for at least 120 min after stimulation (Fig. 4, c and d). This result, taken together with transfection results, and analysis of cells from the proband, confirms that the p.V2013>I mutation confers gain of function on IKK2. These findings are consistent with previous reported results for the same mutation identified as a somatic mutation in patients with central nervous system B cell lymphoma, where gain of function was demonstrated biochemically (Fukumura et al., 2016).

As characterized in the proband, we observed that mice heterozygous and homozygous for $Ikbkb^{V203I}$ exhibited a relative deficiency of T cells (Fig. 4, e and f). T cells were reduced as a

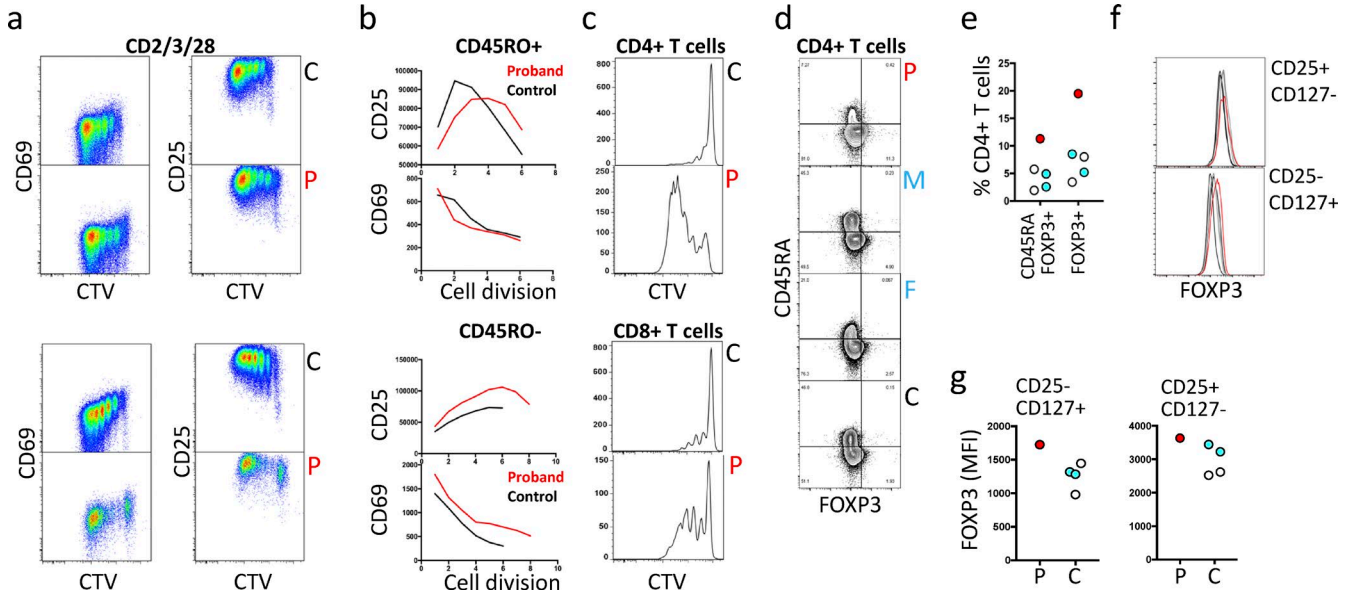

Figure 3. **T cell activation and proliferation. (a)** Flow cytometric analysis of activation and proliferation of CD45RO⁺CD4⁺ T cells (top) and CD45RO⁻CD4⁺ T cells (naive; bottom) stimulated for 6 d with CD2/3/28. Proliferation is indicated by dilution of CTV and activation by expression of CD69 (left) or CD25 (right). Representative of two experiments. **(b)** Number of cells expressing CD69 or CD25 expression according to CD45RO⁺ (top) or CD45RO⁻CD4⁺ T cells (bottom) coexpression. **(c)** CD4⁺ (top) and CD8⁺ (bottom) T cell proliferation determined by dilution of CTV after stimulation with CD3 only. Representative of two experiments. **(d)** T reg cells (FOXP3 vs. CD45RA), gated on CD4⁺ T cells. **(e)** Summary data of activated (CD45RA⁻FOXP3^{hi}) and total T reg cells for patient (red), parents (blue), and healthy controls (open symbols). **(f)** Histograms of FOXP3 expression in cells within the CD127 CD25 gate. Representative of three experiments. Proband, red histogram; parents, black histograms; control, gray histograms. **(g)** Summary data of FOXP3, with summary data of expression level of T reg (CD25⁺CD127⁻) and conventional T cells (CD25⁻CD127⁺) in patient (red), parents (blue), and controls (open symbols). C, healthy control; F, father; M, mother; P, proband.

proportion of splenocytes. We also observed a reduction in absolute number of T cells within spleens of affected mice, and a reduction in absolute numbers of both CD4⁺ and CD8⁺ T cells (Fig. S3), consistent with the human phenotype. In mice, we observed greater reduction in CD8⁺ T cells (Fig. 4 g).

In humans, we observed specific deficiency of naive T cells. In mice, effector T cells are marked by expression of CD44 and absence of CD62L. This subset was increased in both CD4 and CD8 compartments, again with evidence of a gene dose effect (Fig. 4, h and i). We also observed a significant increase in T cell activation, indicated by up-regulation of CD69 in both CD4 and CD8 compartments (Fig. S3, c and d). This bias toward activation was a fixed phenotype, observed in both young and old mice (Fig. S3, e and f). The proband exhibited an increase in circulating T reg cells. In mutant mice, we found an increase in T reg cells defined either according to CD25⁺ surface phenotype or Foxp3 expression (Fig. 4, j and k). A similar increase in T reg cells was observed within thymus of mutant mice, suggesting that the defect arises during T reg cell development (Fig. 4 l).

We have identified a novel germline *IKBKB* allele in patients with a clinical phenotype of cellular abnormalities of lymphopenia combined with immune activation of both CD4⁺ and CD8⁺ T cells. In addition, one patient presented with inflammatory disease and possible ectodermal defect. High evolutionary conservation of the affected codon within *IKBKB* provided us with an opportunity to generate an accurate mouse model of this novel syndrome, which we generated using CRISPR/Cas9 so that they carry the same amino acid substitution in *IKK2* identified in our patient. Phenotypic analysis revealed close phenotypic similarities between mouse and humans carrying the mutant protein, with phenotypes in heterozygotes intermediate between normal and homozygotes, providing strong support for the contention that the novel mutation is responsible for a novel syndrome of immune deficiency (Table 1).

In both human and mouse, we observed pathological immune activation, but this finding needs to be reconciled with clinical manifestation of mild immune deficiency. One possible explanation is the increase in thymic T reg cells, observed in the mouse model, and increased FOXP3 expression in the proband. FOXP3 expression is known to be regulated by canonical NF-κB signaling (Isomura et al., 2009; Long et al., 2009). Furthermore, in loss-of-function defects of canonical NF-κB signaling, concurrent defects in both conventional T cells and T reg cells have been observed, which result in at least partial maintenance of homeostasis be-

Table 1. **Comparison of phenotypes observed in proband and CRISPR/Cas9 *Ikbkb* mutant mouse**

	Human *IKBKB*^{V203I}	**Mouse *Ikbkb*^{V203I}**
CD4⁺ T cells	Reduced	Reduced
CD8⁺ T cells	Reduced	Reduced
B cells	Reduced	Reduced
Memory B cells	Reduced	Reduced
T reg cells	Increased or normal	Increased
T cell activation	Increased (naive)	Increased
Phospho-IκBα	Constitutive activation	Constitutive activation

cause deficiencies of T reg cells are offset by defects in conventional T cell activation conferred by the same mutation (Altin et al., 2011). Patient B.II.1, however, had a late-onset combined immunodeficiency alone and presented with normal T reg cells.

Now that de novo mutations have emerged as important causes of sporadic disease, it is necessary to have methods to confirm causation of novel variants. Our results reveal that even when novel mutations are isolated to a single individual as a result of a de novo mutation, confirmation of function can be confirmed by engineering an orthologous mutation to generate a precise model. This is particularly feasible for immunological diseases, because immunity is highly conserved between mouse and human. In the future, this strategy should prove important for investigating therapeutic interventions for personalized therapy.

Our discovery provides another example of a heterozygous missense mutation in an NF-κB pathway gene that presents with less catastrophic phenotypes than homozygous defects in the same genes. Indeed, given the complex circuits of negative and positive regulatory interactions within NF-κB signaling, cellular, biochemical, and clinical manifestations of specific defects are not always predictable, and complete gene deletions arising spontaneously from nonsense mediated decay or by homologous recombination in mice do not necessarily predict the actions of single–amino acid substitutions. Previously, rare homozygous mutations of *IKBKB* have been reported that result in absence of protein expression and confer severe early onset immune deficiency, in which the cellular phenotype was the opposite of that conferred by the hypermorphic allele reported here, with expansion of naive T cells, which were refractory to activation,

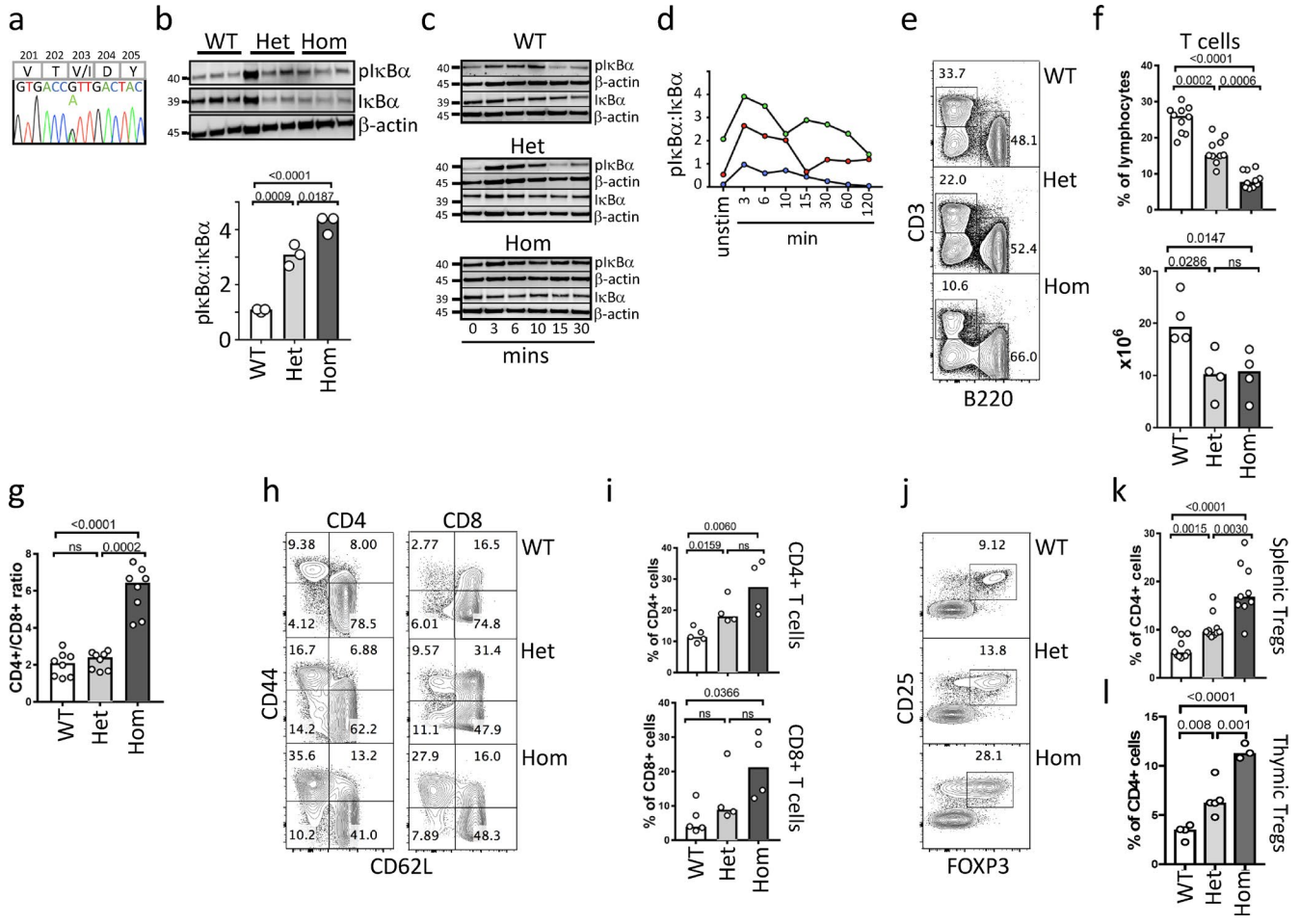

Figure 4. ***Ikbkb* mutation in mouse model. (a)** Sanger sequencing of *Ikbkb* (p.V203>I) from mouse model engineered by CRISPR/Cas9. Translated amino acids are indicated by single letter code. **(b–d)** Phospho-IκBα and total IκBα were compared in splenocytes from age-matched mice heterozygous or homozygous for *Ikbkb* V203>I and their WT littermates at baseline (b) and after activation. Phospho-IκBα and total IκBα at baseline (cells from three mice/genotype shown; b). Ratio of phospho-IκBα (pIκBα) to total IκBα during a time course (c and d), summarized with homozygotes, green; heterozygotes, red; WT, blue. Representative results from three independent experiments. **(e)** Representative plots of relative proportions of B220$^+$ B cells and CD3$^+$ T cells in spleens from WT (upper), heterozygous (*Ikbkb*$^{V203I/+}$; middle), and homozygous (*Ikbkb*$^{V203I/V203I}$; lower) mice. **(f)** CD3$^+$ T cells as a proportion of splenocytes (upper) and absolute counts (lower). **(g)** Ratio of CD4:CD8$^+$ T cells, from heterozygous or homozygous *Ikbkb* mutant mice and their WT littermates. **(h and i)** Representative profiles of CD4$^+$ (left) and CD8$^+$ (right) T cells were analyzed for differentiation according to CD44 and CD62L expression (h). Central memory T cells (CD62L$^+$CD44^{high}) and T_{EM} cells (CD62L^{low}CD44^{high}). Summary of memory T cells (CD44$^+$CD62L^{low}) in CD4$^+$ (upper) and CD8$^+$ cells (lower) compartments (i). **(j–l)** Representative plots of T reg cell subset (CD25$^+$FOXP3$^+$) gated on CD4$^+$ cells from WT (upper), heterozygous (middle), and homozygous (lower) mice (j). T reg summary data from spleen (k) and thymus (l). Each data point represents a single mouse. P values as shown: ns, nonsignificant, as determined by Student's *t* test. Three-way comparisons by ANOVA. Het, heterozygous; Hom, homozygous.

and therefore, there was minimal differentiation of memory or effector T cells. These individuals also exhibit a deficiency of T reg cells (Pannicke et al., 2013; Mousallem et al., 2014). Despite the divergence of cellular phenotypes, we can now conclude that both loss-of-function and hypermorphic alleles of *IKBKB* confer immune deficiency. Similar effects of mutations conferring different biochemical functions have been observed with other genes (Minegishi et al., 2007; Boisson-Dupuis et al., 2012; Haapaniemi et al., 2015). Finally, the relatively mild nature of the phenotype in the patient described here also serves to emphasize that monogenic causes should be considered not only in patients with extreme phenotypes. The corollary is that by elucidating Mendelian versions of less severe phenotypes, we can start to gain insights into the mechanisms of common disease.

Materials and methods

Enrollments and approvals

The family described in this study is part of a larger cohort of primary antibody deficiency kindreds enrolled and recruited through the Australian and New Zealand Antibody Deficiency Allele Study. This study has been approved by human research ethics committees at Australian Capital Territory Health and Australian National University. A Japanese patient was identified from a cohort of Japanese primary immunodeficiency disease. This study was approved by the Ethics Committee of Tokyo Medical and Dental University. All subjects provided written informed consent to participate, in accordance with the Declaration of Helsinki. All animal experiments were approved from the Institutional Animal Ethics Committee of Australian National University in agreement with the code of practice from the National Health and Medical Research Council in Australia.

Flow cytometry and antibodies

The following antibodies were used for human cell analysis: CD19 (SJ25C1), CD27 (L128), CD38 (HB7), CD3 (HIT3A), CD4 (SK3), CD8 (SK1), CCR7 (3D12), CXCR5 (RF8B2), CD24 (ML5), CD69 (FN50), γδTCR, and αβTCR (from BD Biosciences); CD45RA (HI100), CD10 (H110a), CD21 (BU32), and CD45RO (UCHLI; from BioLegend); CD86 (from Miltenyi Biotec); anti-IgM (from Dako); anti-IgD (IAG-2), CD25 Foxp3 (2A3), and phospho-p65 (B33B4WP; from eBioscience); and FOXP3 (259D/C7; from BD Biosciences). The following antibodies were used for mouse flow cytometry analysis: B220 (RA3/6B2), FOXP3 (MF23), and CD127 (A7R34; from eBioscience); and CD3 (17A2), CD4 (RM4-5, GK1.5), CD8 (53/6.7), CD44 (IM7), CD62L (MEL-14), and CD25 (PC61; from BioLegend).

Human PBMCs were isolated by density gradient centrifugation on Ficoll-Paque PLUS (GE Healthcare), washed twice in PBS, and maintained in complete RPMI (Sigma-Aldrich) containing 10% FBS, 2 mM L-glutamine (Sigma-Aldrich), and 100 U/ml penicillin and streptomycin (Sigma-Aldrich). For mouse studies, spleens and thymuses were disrupted to generate single-cell suspensions in RPMI/FCS. For human primary fibroblasts, cells were suspended at a density of 5×10^5 cells/ml in DMEM with 10% FBS.

For surface staining, PBMCs, sorted cells, or mouse cell suspensions were washed with PBS containing 5% FBS (FACS buffer) and then incubated for 20 min at 4°C in dark in FACS buffer containing appropriate fluorochrome-labeled antibodies. Each antibody labeling experiment included an Fc-blocking step (anti-CD16/CD32). Intracellular staining was performed according to standard protocols. Cells were fixed (Fixing Buffer; Thermo Fisher Scientific) and then permeabilized with Perm Buffer III according to the manufacturer's instructions (BD Biosciences).

Proliferation assay

Naive and memory $CD4^+$ or $CD8^+$ T cells were bead sorted (Miltenyi Biotec), and enriched $CD4^+$ or $CD8^+$ cells or PBMCs were cultured with anti-CD3/CD28 expansion beads (Miltenyi Biotec) for 4 or 6 d. Proliferation of cells was then analyzed using Cell Trace Violet Cell Proliferation kit (Invitrogen) according to the manufacturer's instructions.

For CFSE experiments, PBMCs were labeled with 3 µM CFSE (Thermo Fisher Scientific) for 5 min at room temperature. CFSE-labeled cells were plated at 0.5–1.0 × 10^6 cells/ml in triplicate (200 µl/well) in 96-well flat-bottom plates and left unstimulated or stimulated for 7 d with CD40L (1 µg/ml) and CpG (1 µg/ml) for B cell proliferation assay. After staining with fluorochrome-conjugated antibodies, CFSE dilution peaks of $CD19^+$ B cells were analyzed by flow cytometry as a measure of cell division.

CD107a expression analysis

PBMCs were stimulated with staphylococcal enterotoxin B (1 µg/ml) or anti-CD3/CD28 beads in the presence of PE-anti-CD107a (BD Biosciences) and monensin (1 µg/ml) for 6 h and stained for CD8. Cells were analyzed using flow cytometry.

In vitro immunoglobulin production and secretion

PBMCs were stimulated with mitogens (IL-21, 10 ng/ml; CD40L, 2 µg/ml; CpG, 1 µg/ml), and cultured for 11 d. Immunoglobulin levels were evaluated by in-house ELISA assay.

Luciferase assay

Fibroblasts from a healthy control and the patient were transfected with 5 µg NF-κB–dependent firefly luciferase reporter plasmid (pNiFty-Luc) and 0.1 µg of Renilla Luciferase plasmid (pRLC). 20 h after transfection, a portion of the cells were stimulated with 5 ng/ml IL-1B for 4 h. Relative NF-κB activation was measured using Dual-Glo Luciferase Assay System (Promega) and Glomax plate reader (Promega), and it was calculated by normalizing the relative ratio of firefly to Renilla.

Also, the pFN21A expression vector containing WT or mutant *IKBKB*, together with Igkcona-Luc (provided by S. Yamaoka, Tokyo Medical and Dental University, Tokyo, Japan) and pRL-TK (Promega), were transfected into the HEK293T cells. At 24 h after transfection, the cells were treated with TNF-α (20 ng/ml) for 4 h and subjected to luciferase reporter assay. The luciferase assays were performed as described above.

Genotyping and Sanger sequencing

Genomic DNA was isolated either from saliva using Oragene-DNA OG-500 kit (DNAgenoTek) or from blood using the QIAamp DNA Blood kit (QIAGEN) according to the manufacturer's instructions. Genomic DNA was then amplified with primers via a thermocy-

cler. The presence of candidate mutations was then confirmed by Sanger sequencing using Big Dye Terminator v1.1 Sequencing kit (Applied Biosystems), and the amplimers were sent to Biomolecular Resource Facility (Australian National University, Canberra, Australia) to be analyzed by 3730 DNA Analyzer (Applied Biosystems).

Whole exome capture sequencing

For whole exome sequencing, input DNA was extracted from whole blood, analyzed for integrity, and then fragmented by nebulization. DNA library preparation was performed with the Illumina paired-end sample prep kit (Illumina) and followed by exome enrichment (TruSeq Exome Enrichment kit; Illumina). Libraries were sequenced as paired-end reads (100-bp runs) on an Illumina HiSeq 2500.

Analysis comprised alignment of sequences to the human reference sequence GRCh37, using a Burrows-Wheeler aligner (Li and Durbin, 2009). Raw single-nucleotide variants (SNVs) were called against the reference with SAMTools (Li et al., 2009). Common exome variants and deep SNVs were excluded, and coding and splicing variants were captured by alignment with the Ensembl Exomic database. Non-synonymous substitutions were filtered using ANNOVAR. For novel SNVs, prediction of functional effect were done using SIFT (Kumar et al., 2009), PolyPhen-2 (Adzhubei et al., 2010), and Mutation Taster (Schwarz et al., 2014). Filtering of variants for novelty was performed according to the sum of scores for mouse mutant phenotype in the homologous mouse gene, Mendelian disease associations (OMIM), pathway analysis (gene ontology), immune system expression (Immgen), and PolyPhen-2 score. After filtering and ranking variants, heterozygous *IKBKB* variant was investigated further.

Whole exome sequencing data were deposited in the Sequence Read Archive website, accession ID SAMN10107916.

Gene expression

Mutant and WT *IKBKB* mammalian expression constructs pcDNA 3.1(–)/myc-His were obtained from Biomatik, and pFN21A expression vector containing *IKBKB* was purchased from the Promega corporation. The WT and mutant vectors were transfected into HEK293 with Lipofectamine (Invitrogen) and then incubated for 24 h at 37°C with 5% CO_2. Transfectants were stimulated with TNF-α for indicated time.

Western blot

Total protein was extracted from cell line, PBMCs, or mouse spleen cells using radioimmunoprecipitation assay buffer with protease inhibitor cocktail (Roche) and a Halt phosphatase inhibitor (Pierce Net). 25 µg of protein was loaded on a 10% Bolt Bis-Tris PLUS gel (Thermo Fisher Scientific). After separation, proteins were wet-blotted on polyvinylidene fluoride membrane (Bio Rad). Blots were performed with antibodies to phospho-IκBα (Cell Signaling), total IκBα (Cell Signaling), phospho-P100 (Cell Signaling), B-actin (Cell Signaling), and GAPDH (Abcam). Horseradish peroxide–conjugated secondary antibodies were detected with Amersham ELC Western blotting system (GE Healthcare); band intensity was quantitated with Fujifilm multigauge software and normalized to a loading control.

CRISPR/Cas9 mouse construction

Single-guide RNA (sgRNA) design and cloning

For SpCas9 editing, two sgRNAs were designed to ensure a protospacer adjacent motif sequence as close as possible to the desired nucleotide change and to ensure Cas9 endonuclease would generate a double strand break close to the nucleotide of interest, yielding the following sgRNAs: guide 1, 5′-CTCCAGTAGTCAACG GTCACGG-3′ and guide 2, 5′-TACTGGAGCTTCGGCACCCTGG-3′. No significant off-target effects were detected by in silico analysis (CCTop software; Stemmer et al., 2015). A single-stranded oligonucleotide (ssODN) template was chemically synthetized as a 4 nM ultramer oligonucleotide from IDT with the following sequence: ssOdn1 5′-ACCTTGGAAGGTGTGTCTGGGCTGAGGGGA GAAGGCATGAGGCTTGACTCTCCCCTGTTCCCTAGCAGAGGTGAA AGAAGGCAGTGCCTATGGGAGCCAGTCAGTGGAGCAGGAGGC AGAGAAGCTGTGTCCACCCCCTGAGCCTCCAGGAGGGCTCTGCCA CGGGCA-3′. For sgRNA synthesis, a 455-bp vector was designed including a U6 promoter with a sgRNA, TracRNA scaffold, and a termination signal. The sgRNA was chemically synthetized as a gBlocks gene fragment (IDT), adapted from Mali et al. (2013). The sequences are as follows: for guide 1, 5′-TGTACAAAAAAGCAG GCTTTAAAGGAACCAATTCAGTCGACTGGATCCGGTACCAAGGTC GGGCAGGAAGAGGGCCTATTTCCCATGATTCCTTCATATTTGCAT ATACGATACAAGGCTGTTAGAGAGATAATTAGAATTAATTTGACT GTAAACACAAAGATATTAGTACAAAATACGTGACGTAGAAAGTAA TAATTTCTTGGGTAGTTTGCAGTTTTAAAATTATGTTTTAAAATG GACTATCATATGCTTACCGTAACTTGAAAGTATTTCGATTTCTTG GCTTTATATATCTTGTGGAAAGGACGAAACACCGCTCCAGTAGTC AACGGTCAGTTTTAGAGCTAGAAATAGCAAGTTAAAATAAGGCTA GTCCGTTATCAACTTGAAAAAGTGGCACCGAGTCGGTGCTTTTTT TCTAGACCCAGCTTTCTTGTACAAAGTTGGCATTA-3′; and guide 2, 5′-TGTACAAAAAAGCAGGCTTTAAAGGAACCAATTCAGTCGACT GGATCCGGTACCAAGGTCGGGCAGGAAGAGGGCCTATTTCCC ATGATTCCTTCATATTTGCATATACGATACAAGGCTGTTAGAGAG ATAATTAGAATTAATTTGACTGTAAACACAAAGATATTAGTACAA AATACGTGACGTAGAAAGTAATAATTTCTTGGGTAGTTTGCAGTT TTAAAATTATGTTTTAAAATGGACTATCATATGCTTACCGTAACT TGAAAGTATTTCGATTTCTTGGCTTTATATATCTTGTGGAAAGGA CGAAACACCGTACTGGAGCTTCGGCACCCGTTTTAGAGCTAGAAA TAGCAAGTTAAAATAAGGCTAGTCCGTTATCAACTTGAAAAAGTG GCACCGAGTCGGTGCTTTTTTTCTAGACCCAGCTTTCTTGTACAA AGTTGGCATTA-3′. 100 ng of synthetized gBlock gene fragment was Topo TA–cloned into a pCR2.1TOPO vector (Thermo Fisher Scientific), and the cloned fragments were Ampicillin-selected according to the manufacturer's instructions. The vector was transformed into *Escherichia coli* (Thermo Fisher Scientific).

Mouse husbandry and zygotes microinjection

C57BL6/Ncrl and Swiss Webster CFW/crl recipient mice (Charles River) were maintained at the Australian Phenomics Facility under specific pathogen–free conditions. 5-wk-old C57BL/6Ncrl females were superovulated then mated with 20-wk-old C57BL/6Ncrl stud males. Fertilized zygotes were collected from the oviduct and maintained under M16 medium (M7292; Sigma-Aldrich) overlaid with mineral oil. A mix of 50 ng/µl of SpCas9 protein (PNA Bio), *Ikbk*-purified gBlocks plasmids (guide 1, 5 ng/µl and guide 2, 5 ng/µl), and 100 ng/µl of ssODN

suspended into nuclease-free water (Thermo Fisher Scientific) were coinjected into the mouse zygotes. Pronuclear injections were performed in a M2 medium (M7167; Sigma-Aldrich) overlaid with mineral oil under a DMi8 (Leica) inverted microscope apparatus associated with mechanical micromanipulators and a microinjection apparatus. Microinjected zygotes were cultured overnight at 37°C in a 5% CO_2 incubator and then surgically transferred at two-cell stage into the ampulla of CFW/crl pseudo-pregnant females.

Genotyping

DNA extraction was performed on ear punches lysed in Tris-EDTA-Tween lysis buffer (50 mM Tris HCl, pH 8.0, 0.125 mM EDTA, and 2% Tween 20, plus proteinase K) and incubated at 56°C for 1 h before the DNA was denatured at 95°C for 10 min. Genotyping primers were as follows: SF, 5′-TTCCTCTCCTCACACCCAAG-3′ and 5′-ATTGAACAAGAGTGGTCGCC-3′. The Sanger sequencing was performed in the Biomolecular Resource facilities at the Australian National University.

Protein structure

The structure data of the human IKK2 protein (PDB code: 4KIK) was used. The structures of the mutants, p.K171E and p.V203I, of IKK2 protein were built with the Molecular Operating Environment software (2013.08; Chemical Computing Group Inc.), and the structural figures were prepared.

Statistical analysis

Student's *t* test, ANOVA, and χ^2 tests were used to determine the statistical significance, which was set at the 95% confidence level.

Online supplemental material

Table S1 summarizes clinical results for patients. Fig. S1 shows conservation and function of IKK2 mutation. Fig. S2 shows human lymphocyte function and phenotype. Fig. S3 shows T cell phenotype in *Ikbkb*^{V203I} mice.

Acknowledgments

The authors thank Anastasia Wilson, Ann-Maree Hatch, Yafei Zhang, Wesley Lam, Yuichi Shiraisih, Kenichi Chiba, Hiroko Tanaka, and Hideki Muramatsu for their technical assistance in the conduct of the study. We thank our colleagues at the Centre for Personalised Immunology and Dr. Bodo Grimbacher from Freiburg University for helpful discussions and feedback on the study. We are grateful to our patients and their families for their willing participation in the research.

The study was funded by National Health and Medical Research Council grants 1107464 (to M.C. Cook), 1079648 (to C.G. Vinuesa and M.C. Cook), and 1113577 (to C.G. Vinuesa and M.C. Cook); The Bev and Alan Harvey Bequest; Japan Society for the Promotion of Science grants KAKENHI JP16H05355 (to S. Okada), 16K15528 (to S. Okada), JP26461570 (to H. Kanegane), and JP17K10099 (to H. Kanegane); and the Practical Research Project for Rare/Intractable Diseases from the Japan Agency for Medical Research and Development.

The authors declare no competing financial interests.

Author contributions: C. Cardinez, B. Miraghazadeh, K. Tanita, A. Hoshino, and E. da Silva performed cellular and biochemical phenotyping experiments. S. Okada performed the luciferase reporter assays. R. Chand performed flow cytometry. T. Asano and M. Tsumura performed additional immunological studies. K. Yoshida, Y. Okuno, S. Miyano, and S. Ogawa performed whole exome sequencing. M. Yamazaki provided clinical samples and data. Z. Kato and H. Ohnishi undertook structural analysis. T.D. Andrews and M.A. Field performed bioinformatic analysis. G. Burgio generated the CRISPR/Cas9 mouse strain. T. Morio, C.G. Vinuesa, H. Kanegane, and M.C. Cook supervised the study. C. Cardinez, B. Miraghazadeh, K. Tanita, S. Kojima, H. Kanegane, and M.C. Cook wrote the manuscript.

Submitted: 4 April 2018
Revised: 27 June 2018
Accepted: 24 September 2018

References

Adzhubei, I.A., S. Schmidt, L. Peshkin, V.E. Ramensky, A. Gerasimova, P. Bork, A.S. Kondrashov, and S.R. Sunyaev. 2010. A method and server for predicting damaging missense mutations. *Nat. Methods.* 7:248–249. https://doi.org/10.1038/nmeth0410-248

Altin, J.A., L. Tian, A. Liston, E.M. Bertram, C.C. Goodnow, and M.C. Cook. 2011. Decreased T-cell receptor signaling through CARD11 differentially compromises forkhead box protein 3-positive regulatory versus T(H)2 effector cells to cause allergy. *J. Allergy Clin. Immunol.* 127:1277–85.e5. https://doi.org/10.1016/j.jaci.2010.12.1081

Baeuerle, P.A., and D. Baltimore. 1988. I kappa B: a specific inhibitor of the NF-kappa B transcription factor. *Science.* 242:540–546. https://doi.org/10.1126/science.3140380

Bohuslav, J., V.V. Kravchenko, G.C. Parry, J.H. Erlich, S. Gerondakis, N. Mackman, and R.J. Ulevitch. 1998. Regulation of an essential innate immune response by the p50 subunit of NF-kappaB. *J. Clin. Invest.* 102:1645–1652. https://doi.org/10.1172/JCI3877

Boisson-Dupuis, S., X.-F. Kong, S. Okada, S. Cypowyj, A. Puel, L. Abel, and J.-L. Casanova. 2012. Inborn errors of human STAT1: allelic heterogeneity governs the diversity of immunological and infectious phenotypes. *Curr. Opin. Immunol.* 24:364–378. https://doi.org/10.1016/j.coi.2012.04.011

Conley, M.E., and J.-L. Casanova. 2014. Discovery of single-gene inborn errors of immunity by next generation sequencing. *Curr. Opin. Immunol.* 30:17–23. https://doi.org/10.1016/j.coi.2014.05.004

Fan, C.-M., and T. Maniatis. 1991. Generation of p50 subunit of NF-kappa B by processing of p105 through an ATP-dependent pathway. *Nature.* 354:395–398. https://doi.org/10.1038/354395a0

Field, M.A., V. Cho, T.D. Andrews, and C.C. Goodnow. 2015. Reliably Detecting Clinically Important Variants Requires Both Combined Variant Calls and Optimized Filtering Strategies. *PLoS One.* 10:e0143199. https://doi.org/10.1371/journal.pone.0143199

Flanagan, S.E., E. Haapaniemi, M.A. Russell, R. Caswell, H.L. Allen, E. De Franco, T.J. McDonald, H. Rajala, A. Ramelius, J. Barton, et al. 2014. Activating germline mutations in STAT3 cause early-onset multi-organ autoimmune disease. *Nat. Genet.* 46:812–814. https://doi.org/10.1038/ng.3040

Fukumura, K., M. Kawazu, S. Kojima, T. Ueno, E. Sai, M. Soda, H. Ueda, T. Yasuda, H. Yamaguchi, J. Lee, et al. 2016. Genomic characterization of primary central nervous system lymphoma. *Acta Neuropathol.* 131:865–875. https://doi.org/10.1007/s00401-016-1536-2

Haapaniemi, E.M., M. Kaustio, H.L.M. Rajala, A.J. van Adrichem, L. Kainulainen, V. Glumoff, R. Doffinger, H. Kuusanmäki, T. Heiskanen-Kosma, L. Trotta, et al. 2015. Autoimmunity, hypogammaglobulinemia, lymphoproliferation, and mycobacterial disease in patients with activating mutations in STAT3. *Blood.* 125:639–648. https://doi.org/10.1182/blood-2014-04-570101

Häcker, H., and M. Karin. 2006. Regulation and function of IKK and IKK-related kinases. *Sci. STKE.* 2006:re13. https://doi.org/10.1126/stke.3572006re13

Hayden, M.S., and S. Ghosh. 2004. Signaling to NF-kappaB. *Genes Dev.* 18:2195–2224. https://doi.org/10.1101/gad.1228704

Isomura, I., S. Palmer, R.J. Grumont, K. Bunting, G. Hoyne, N. Wilkinson, A. Banerjee, A. Proietto, R. Gugasyan, L. Wu, et al. 2009. c-Rel is required for the development of thymic Foxp3+ CD4 regulatory T cells. *J. Exp. Med.* 206:3001–3014. https://doi.org/10.1084/jem.20091411

Kataoka, K., Y. Nagata, A. Kitanaka, Y. Shiraishi, T. Shimamura, J. Yasunaga, Y. Totoki, K. Chiba, A. Sato-Otsubo, G. Nagae, et al. 2015. Integrated molecular analysis of adult T cell leukemia/lymphoma. *Nat. Genet.* 47:1304–1315. https://doi.org/10.1038/ng.3415

Kumar, P., S. Henikoff, and P.C. Ng. 2009. Predicting the effects of coding non-synonymous variants on protein function using the SIFT algorithm. *Nat. Protoc.* 4:1073–1081. https://doi.org/10.1038/nprot.2009.86

Li, H., and R. Durbin. 2009. Fast and accurate short read alignment with Burrows-Wheeler transform. *Bioinformatics.* 25:1754–1760. https://doi.org/10.1093/bioinformatics/btp324

Li, H., B. Handsaker, A. Wysoker, T. Fennell, J. Ruan, N. Homer, G. Marth, G. Abecasis, and R. Durbin. 1000 Genome Project Data Processing Subgroup. 2009. The Sequence Alignment/Map format and SAMtools. *Bioinformatics.* 25:2078–2079. https://doi.org/10.1093/bioinformatics/btp352

Liu, S., Y.R. Misquitta, A. Olland, M.A. Johnson, K.S. Kelleher, R. Kriz, L.L. Lin, M. Stahl, and L. Mosyak. 2013. Crystal structure of a human IκB kinase β asymmetric dimer. *J. Biol. Chem.* 288:22758–22767. https://doi.org/10.1074/jbc.M113.482596

Long, M., S.-G. Park, I. Strickland, M.S. Hayden, and S. Ghosh. 2009. Nuclear factor-kappaB modulates regulatory T cell development by directly regulating expression of Foxp3 transcription factor. *Immunity.* 31:921–931. https://doi.org/10.1016/j.immuni.2009.09.022

Mali, P., L. Yang, K.M. Esvelt, J. Aach, M. Guell, J.E. DiCarlo, J.E. Norville, and G.M. Church. 2013. RNA-guided human genome engineering via Cas9. *Science.* 339:823–826. https://doi.org/10.1126/science.1232033

Minegishi, Y., M. Saito, S. Tsuchiya, I. Tsuge, H. Takada, T. Hara, N. Kawamura, T. Ariga, S. Pasic, O. Stojkovic, et al. 2007. Dominant-negative mutations in the DNA-binding domain of STAT3 cause hyper-IgE syndrome. *Nature.* 448:1058–1062. https://doi.org/10.1038/nature06096

Mousallem, T., J. Yang, T.J. Urban, H. Wang, M. Adeli, R.E. Parrott, J.L. Roberts, D.B. Goldstein, R.H. Buckley, and X.-P. Zhong. 2014. A nonsense mutation in IKBKB causes combined immunodeficiency. *Blood.* 124:2046–2050. https://doi.org/10.1182/blood-2014-04-571265

Pannicke, U., B. Baumann, S. Fuchs, P. Henneke, A. Rensing-Ehl, M. Rizzi, A. Janda, K. Hese, M. Schlesier, K. Holzmann, et al. 2013. Deficiency of innate and acquired immunity caused by an IKBKB mutation. *N. Engl. J. Med.* 369:2504–2514. https://doi.org/10.1056/NEJMoa1309199

Picard, C., H. Bobby Gaspar, W. Al-Herz, A. Bousfiha, J.-L. Casanova, T. Chatila, Y.J. Crow, C. Cunningham-Rundles, A. Etzioni, J.L. Franco, et al. 2018. International Union of Immunological Societies: 2017 Primary Immunodeficiency Diseases Committee Report on Inborn Errors of Immunity. *J. Clin. Immunol.* 38:96–128. https://doi.org/10.1007/s10875-017-0464-9

Plaksin, D., P.A. Baeuerle, and L. Eisenbach. 1993. KBF1 (p50 NF-kappa B homodimer) acts as a repressor of H-2Kb gene expression in metastatic tumor cells. *J. Exp. Med.* 177:1651–1662. https://doi.org/10.1084/jem.177.6.1651

Salmerón, A., J. Janzen, Y. Soneji, N. Bump, J. Kamens, H. Allen, and S.C. Ley. 2001. Direct phosphorylation of NF-kappaB1 p105 by the IkappaB kinase complex on serine 927 is essential for signal-induced p105 proteolysis. *J. Biol. Chem.* 276:22215–22222. https://doi.org/10.1074/jbc.M101754200

Scheidereit, C. 2006. IkappaB kinase complexes: gateways to NF-kappaB activation and transcription. *Oncogene.* 25:6685–6705. https://doi.org/10.1038/sj.onc.1209934

Schwarz, J.M., D.N. Cooper, M. Schuelke, and D. Seelow. 2014. D.S.N. methods. MutationTaster2: mutation prediction for the deep-sequencing age. *Oncogene.* https://doi.org/10.1038/nmeth.2890

Snow, A.L., W. Xiao, J.R. Stinson, W. Lu, B. Chaigne-Delalande, L. Zheng, S. Pittaluga, H.F. Matthews, R. Schmitz, S. Jhavar, et al. 2012. Congenital B cell lymphocytosis explained by novel germline CARD11 mutations. *J. Exp. Med.* 209:2247–2261. https://doi.org/10.1084/jem.20120831

Staudt, L.M. 2010. Oncogenic activation of NF-kappaB. *Cold Spring Harb. Perspect. Biol.* 2:a000109. https://doi.org/10.1101/cshperspect.a000109

Stemmer, M., T. Thumberger, M. Del Sol Keyer, J. Wittbrodt, and J.L. Mateo. 2015. CCTop: An Intuitive, Flexible and Reliable CRISPR/Cas9 Target Prediction Tool. *PLoS One.* 10:e0124633. https://doi.org/10.1371/journal.pone.0124633

Stepensky, P., B. Keller, M. Buchta, A.-K. Kienzler, O. Elpeleg, R. Somech, S. Cohen, I. Shachar, L.A. Miosge, M. Schlesier, et al. 2013. Deficiency of caspase recruitment domain family, member 11 (CARD11), causes profound combined immunodeficiency in human subjects. *J. Allergy Clin. Immunol.* 131:477–85.e1. https://doi.org/10.1016/j.jaci.2012.11.050

Vissers, L.E.L.M., J. de Ligt, C. Gilissen, I. Janssen, M. Steehouwer, P. de Vries, B. van Lier, P. Arts, N. Wieskamp, M. del Rosario, et al. 2010. A de novo paradigm for mental retardation. *Nat. Genet.* 42:1109–1112. https://doi.org/10.1038/ng.712

Weih, F., D. Carrasco, S.K. Durham, D.S. Barton, C.A. Rizzo, R.P. Ryseck, S.A. Lira, and R. Bravo. 1995. Multiorgan inflammation and hematopoietic abnormalities in mice with a targeted disruption of RelB, a member of the NF-kappa B/Rel family. *Cell.* 80:331–340. https://doi.org/10.1016/0092-8674(95)90416-6

Woyach, J.A., A.J. Johnson, and J.C. Byrd. 2012. The B-cell receptor signaling pathway as a therapeutic target in CLL. *Blood.* 120:1175–1184. https://doi.org/10.1182/blood-2012-02-362624

Zhang, Q., M.J. Lenardo, and D. Baltimore. 2017. 30 Years of NF-κB: A Blossoming of Relevance to Human Pathobiology. *Cell.* 168:37–57. https://doi.org/10.1016/j.cell.2016.12.012